Strain effect on self-diffusion in silicon: Numerical study

P. Ganster, G. Tréglia, and A. Saúl*
CINAM-CNRS, Aix-Marseille Université, Campus de Luminy, Case 913, F13288 Marseille Cedex 9, France
(Received 15 July 2008; revised manuscript received 6 February 2009; published 11 March 2009)

We present here a numerical study of the self-diffusion mechanisms in silicon using a semiempirical Stillinger-Weber potential to calculate formation and migration energies and entropies. We find that self-diffusion in bulk Si is mediated by vacancies at low temperature, but that interstitials play a more and more important role when temperature increases, in agreement with recent experimental data. This behavior is shown to strongly evolve under biaxial strain (ϵ) which simulates the effect of epitaxial growth of a Si thin film. Our methodology allows us to classify vacancy vs interstitial self-diffusion within a (T,ϵ) diagram, which reveals a transition from vacancy toward interstitial diffusion at low temperature beyond a critical tensile strain which corresponds to Si/Ge size mismatch.

DOI: 10.1103/PhysRevB.79.115205 PACS number(s): 61.72.Bb, 66.10.cg, 87.16.A−

I. INTRODUCTION

Intrinsic point defects in silicon have been the subject of many experimental and theoretical studies from both fundamental and technological points of view. Indeed, the presence of these defects can induce electronic states inside the band gap, which perturb or enhance the electronic characteristics of the device depending on that they are mastered or not. In this framework, a deep understanding of the Si self-diffusion mechanism, which is essential in the impurity diffusion or the annealing of implantation damages, is required for the development of process simulators for nano-Si electronics. To this aim, one has to keep in mind that most Si materials used in the latter case are thin films, which suffer various types of strains (e.g., induced by epitaxial growth on a substrate presenting a large size mismatch). In that case, self-diffusion mechanisms are expected to differ from what they are in bulk Si and it is essential to understand how they will evolve depending on the sign (tensile, compressive) of the strain.

Unfortunately, although it is experimentally possible to detect Si vacancies using EPR or positron-lifetime experiments,[1–3] the situation is worse for Si self-interstitials which cannot be detected directly. The alternative is then to rely on numerical simulations to elucidate the atomistic nature of the efficient defects. Thus many theoretical investigations have been devoted during the last decades to the study of self-diffusion in bulk silicon using either empirical potentials[4–10] or *ab initio* methods.[11–27]

However, in most cases the authors focused on the energetic part of the diffusion coefficient, namely, the formation and/or migration energies of point defects, only a few of them considering the formation entropies and diffusivity prefactors as possible key factors of the self-diffusion process. Moreover in the latter case, it is rather difficult to find a consensus on the formation entropy, which can perhaps be related to the different methodologies used by the authors to determine the various contributions. Indeed, only a few studies have been reported in which all the (energetic, entropic) contributions to the diffusion coefficient have been calculated in the framework of the same description of the interatomic interactions. Among them, let us mention the work by Sinno *et al.*[28] who considered carefully these topics within Stillinger-Weber (SW) potential[29] but did not show the final result for the self-diffusion coefficient. Finally no theoretical atomistic study of the influence of stress on these self-diffusion mechanisms has been performed up to now.

Our goal here is to present a study of the influence of a biaxial strain, which could mimic the effect of epitaxy for a thin Si film, on self-diffusion in silicon, using the semiempirical SW potential. To this aim, the paper is organized as follows. First, we introduce the fundamental concepts of the self-diffusion and the methods to calculate the physical quantities which govern it. Then we give details on the criteria we use to choose our potential. In Sec. III, we compare vacancy and interstitial self-diffusion mechanisms in bulk Si, with particular emphasis on the influence of temperature on their respective efficiencies. Finally, in Sec. IV, we use the methodology developed in the previous sections to illustrate the influence of a biaxial strain on these diffusion mechanisms. The key point of the paper is then the elaboration of a (T,ϵ) diagram which allows us to classify vacancy vs interstitial self-diffusion as a function of temperature (T) and strain (ϵ) and which reveals in particular a transition in the diffusion behavior beyond a critical tensile strain which corresponds to Si/Ge size mismatch.

II. SI SELF-DIFFUSION MODEL

Diffusion proceeds through the formation and migration of defects (def), the nature of which depends on the material under consideration. Thus, although the single defect involved in metal diffusion is the vacancy (V), various types of interstitials (I) can also play a role in semiconductor diffusion. The most common defects are shown in Fig. 1.

In any case, if one assumes that the different mechanisms are independent from one another, the global or total diffusion coefficient at temperature T can be written[30] as

$$D(T) = \sum_{\text{def}} c^{\text{def}}(T) D^{\text{def}}(T) = \sum_{\text{def}} c^{\text{def}}(T) f^{\text{def}}(T) d^{\text{def}}(T), \quad (1)$$

where $c^{\text{def}}(T)$ is the equilibrium concentration of the defect at temperature T and $D^{\text{def}}(T)$ is the self-diffusion diffusivity due to the presence of the defect. The latter can be written as the

 ©2009 The American Physical Society

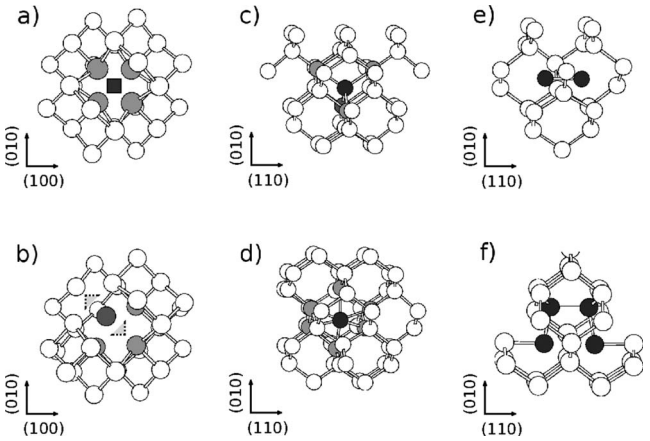

FIG. 1. Defects in silicon, (a) the single vacancy located on a single site or (b) split between two sites, and various interstitials (c) tetrahedral, (d) hexagonal, (e) ⟨110⟩ dumbbell, and (f) ⟨110⟩ extended dumbbell.

product of the individual mobility of the considered single defect $d^{\mathrm{def}}(T)$ and the correlation factor $f^{\mathrm{def}}(T)$ which accounts for the fact that successive atom jumps can be related to one another so that the atoms do not follow a strict uncorrelated random walk but a correlated one. Calculating these correlation factors is not an easy task because it depends on the temperature, the diffusion mechanism, and on the lattice geometry. For diamond-type structures, it is generally assumed that it is equal to 0.5 for a vacancy and to 0.727 for interstitials.[31] In fact, recent calculations performed within a SW potential showed that it varies for the different types of interstitials displayed in Fig. 1, and that it is closer to 0.6 for the dumbbell mechanism which prevails with this potential.[8] The method used in this work (see below) will give us directly diffusivity coefficient due to the presence of the defect $D^{\mathrm{def}}(T)$, whereas a more sophisticated method should be used to calculate separately f^{def} and d^{def}.[8,9]

In Secs. II A and II B we will define the methodology that we have followed to calculate each contribution, assuming a choice of a suited interatomic potential. The strategy that we have followed to chose the potential will be explained in Sec. II C.

A. Formation of point defects

The defect formation is a thermally activated process, which follows an Arrhenius-type behavior

$$c^{\mathrm{def}}(T) = \exp\left[\frac{\Delta S_f^{\mathrm{def}}}{k_B}\right]\exp\left[-\frac{\Delta E_f^{\mathrm{def}}}{k_B T}\right], \tag{2}$$

where k_B is the Boltzmann constant, $\Delta E_f^{\mathrm{def}}$ is the formation energy, and $\Delta S_f^{\mathrm{def}}$ the formation entropy.

$\Delta E_f^{\mathrm{def}}$ is the energy required to create the point defect. More precisely, the vacancy formation energy ΔE_f^V is the energy involved when one atom is removed from an initially perfect crystalline box and placed in a *reservoir*. Similarly, the interstitial formation energy ΔE_f^I is defined as the energy involved when an atom from the reservoir is added to a perfect crystalline box. The atoms in the reservoir are assumed to have the cohesive energy of the perfect crystal.

The formation entropy $\Delta S_f^{\mathrm{def}}$ refers to the phase-space volume accessible to the defect. It involves two contributions, respectively, of configurational and vibrational origins

$$\Delta S_f^{\mathrm{def}} = \Delta S_{f,\mathrm{conf}}^{\mathrm{def}} + \Delta S_{f,\mathrm{vib}}^{\mathrm{def}}. \tag{3}$$

The configurational part is purely geometrical since it is related to the number of ways the defect can exist in one particular lattice site. It is equal to $k_B \ln 3$ for a vacancy due to the three possible orientations made available by Jahn-Teller effect[24] and equal to $k_B \ln 6$ for the split interstitial or dumbbell (see Fig. 1).[13] However, this does not hold when using semiempirical potentials, such as the SW potential, which do not account for Jahn-Teller effect, so that in that case $\Delta S_{f,\mathrm{conf}}^V = 0$. In order to be consistent, we will use this zero value in the following.

The vibrational part of the formation entropy $\Delta S_{f,\mathrm{vib}}^{\mathrm{def}}$ is defined and calculated from the same balance as the formation energy, namely, as the difference in total vibrational entropy between an initially perfect crystalline box and a final defective one; the removed or added atom being located at a perfect bulk position

$$\Delta S_{f,\mathrm{vib}}^{\mathrm{def}} = \int_0^\infty [n^{\mathrm{def}}(\nu) - n^0(\nu)] g(\nu) d\nu, \tag{4}$$

where $n^{\mathrm{def}}(\nu)$ is the total phonon density of states (DOS) of the defective system, $n^0(\nu)$ is the density of states of a perfect system having the same number of atoms, $g(\nu)$ the contribution to the entropy of a single mode

$$g(\nu) = \frac{h\nu}{2T}\coth\left(\frac{h\nu}{2k_B T}\right) - k_B \ln\left[2 \sinh\left(\frac{h\nu}{2k_B T}\right)\right], \tag{5}$$

and h the Planck constant. The vibrational density of states $n(\nu)$ is calculated via the dynamical matrix method in the harmonic approximation (at 0 K). More precisely, the vibrational frequencies and the corresponding eigenmodes are obtained by diagonalizing the dynamical matrix, first in the perfect system and then in the one containing a point defect (vacancy or interstitial).

The total densities of states can be decomposed into projected densities of states (PDOSs) or partial site contributions at site i and direction α,

$$n(\nu) = \sum_{i,\alpha}^{3N} n_{i\alpha}(\nu). \tag{6}$$

In practice, it is sufficient to calculate these PDOSs for the Z^{def} sites surrounding the defect which feel its influence. The vibrational contribution to the formation entropy becomes

$$\Delta S_{f,\mathrm{vib}}^{\mathrm{def}} \approx \int_0^\infty \sum_{i,\alpha}^{3Z^{\mathrm{def}}} [n_{i\alpha}^{\mathrm{def}}(\nu) - n_{i\alpha}^0(\nu)] g(\nu) d\nu. \tag{7}$$

A further approximation can be made in the limit of high temperature where $g(\nu)$ reduces to $-k_B \ln(h\nu/k_B T)$. In this limit a single average Einstein frequency can be used to characterize the perfect system

$$\bar{\nu}^0 = \frac{1}{3Z^{\text{def}}} \sum_{i,\alpha}^{3Z^{\text{def}}} \int_0^\infty \nu n_{i\alpha}^0(\nu) d\nu, \tag{8}$$

a different one for the defective system

$$\bar{\nu}^{\text{def}} = \frac{1}{3Z^{\text{def}}} \sum_{i,\alpha}^{3Z^{\text{def}}} \int_0^\infty \nu n_{i\alpha}^{\text{def}}(\nu) d\nu$$

$$= \bar{\nu}^0 + \frac{1}{3Z^{\text{def}}} \sum_{i,\alpha}^{3Z^{\text{def}}} \int_0^\infty \nu [n_{i\alpha}^{\text{def}}(\nu) - n_{i\alpha}^0(\nu)] d\nu, \tag{9}$$

and the formation entropy given by Eq. (7) reduces to a simple analytical expression

$$\Delta S_{f,\text{vib}}^{\text{def}} \approx 3Z^{\text{def}} k_B \ln\left(\frac{\bar{\nu}^0}{\bar{\nu}^{\text{def}}}\right) \approx 3Z^{\text{def}} k_B \frac{\bar{\nu}^0 - \bar{\nu}^{\text{def}}}{\bar{\nu}^0}, \tag{10}$$

which has the advantage to allow guessing the behavior of this term from the main variations of the local density induced by the presence of the defect, i.e., deformation toward low or high frequencies depending on the compressive or tensile stress.

B. Migration of point defects

Migration is also a thermally activated process

$$D^{\text{def}}(T) = D_m^{\text{def}} \exp\left[-\frac{\Delta E_m^{\text{def}}}{k_B T}\right]. \tag{11}$$

Here ΔE_m^{def} is the defect migration energy (barrier) and D_m^{def} the corresponding prefactor which in the simplest approximation is directly related to the jump frequency of the defect from one site to another multiplied by the correlation factor.

1. Static calculation

Concerning the migration energy its calculation is rather easy once the saddle point has been properly identified. It is defined as the difference in total energies of a system in which the defect occupies the saddle point or the stable positions. However, despite the availability of "static" methods such as the "nudged elastic band"[32] or "activation-relaxation technique"[33] to sample energy barriers and migration paths, their determination is difficult and computationally expensive when the potential-energy landscape is complex,[10,27] which is the case for interstitials since the migration path contains multiple minima.[20]

A static determination of the diffusivity or migration prefactor D_m^{def} can be performed using the following expression:

$$D_m^{\text{def}} = g^{\text{def}} f^{\text{def}} a^2 \nu_0^{\text{def}} \exp\left(\frac{\Delta S_{m,\text{vib}}^{\text{def}}}{k_B}\right), \tag{12}$$

where $\Delta S_{m,\text{vib}}^{\text{def}}$ is the migration entropy,[34,35] a is the cubic lattice parameter, g^{def} a geometrical factor, and ν_0^{def} is the average vibration frequency of an atom first neighbor of the defect. This average frequency accounts for the number of attempts made by the atom per unit time to cross the barrier to the vacancy. For the sake of simplicity, we will assume here that $\nu_0^{\text{def}} = \bar{\nu}^{\text{def}}$ [see Eq. (9)]. The geometrical factor g^{def} accounts for the number of possible intermediate states between the initial and final configurations.[31] It depends in principle on the nature of the defect:[31,36] it is equal to 1/4 for point interstitials such as those shown in Figs. 1(c) and 1(d) and equal to 1/8 both for the vacancy [Fig. 1(a)] and the ⟨110⟩ extended dumbbell interstitial [Fig. 1(f)].

The migration entropy is defined similarly to the migration energy, as the difference in entropy between systems in which the defects occupy stable or saddle-point positions. The entropic terms can be calculated once again through Eqs. (6) and (7) from the phonon densities around the defect in both positions (stable and saddle point) using the numerical procedure already described. Similarly to the formation energy, in the high-temperature limit the migration entropy can be written simply as

$$\Delta S_{m,\text{vib}}^{\text{def}} \approx (3Z^{\text{def}} - 1) k_B \ln\left(\frac{\bar{\nu}^{\text{def}}}{\bar{\nu}^{\text{def}*}}\right), \tag{13}$$

where $\bar{\nu}^{\text{def}*}$ is the average value of the phonon DOS with the system in the saddle-point position. The factor $(3Z^{\text{def}} - 1)$ instead of $3Z^{\text{def}}$ as in Eq. (10) comes from the existence of an imaginary frequency in the phonon DOS at the unstable saddle point. If both average frequencies do not differ too much, the migration entropy vanishes and a simplified expression of the prefactor is recovered[36]

$$D_m^{\text{def}} \approx g^{\text{def}} f^{\text{def}} a^2 \bar{\nu}^{\text{def}}. \tag{14}$$

2. Dynamic calculation

A way to avoid the difficulties encountered using static methods, which require a perfect knowledge of the correlation factor and of the saddle-point positions, is to calculate directly the diffusivity, i.e., at the same time the energy barrier and the prefactor. This can be achieved by performing molecular-dynamics calculations at different temperatures in a system which contains the point defect under study. During the self-diffusion process, the square displacement at temperature T is related to the diffusivity via the Einstein's law

$$\sum_{i=1}^{N\pm 1} |r_i(t) - r_i(0)|^2 \sim 6D^{\text{def}}(T) t, \tag{15}$$

where t is the simulation time, $r_i(t)$ is the atomic position of atom i, and $D^{\text{def}}(T)$ is the diffusivity coefficient defined in Eq. (1) which according to Eq. (11) follows an Arrhenius behavior. The numerical protocol used to calculate $D^{\text{def}}(T)$ from dynamical simulations will be detailed in Sec. III.

C. Choice of the Si potential

In the literature, there are many interatomic potentials for Si which have been developed to tackle different physical quantities. Unfortunately, in most cases they have been developed without paying special attention to the point defects. A nice review which discusses critically the abilities of various empirical potentials to account for the energetic characteristics of silicon was published by Balamane *et al.*[37] We

TABLE I. Formation energy of silicon point defects (vacancy V, split vacancy SV, tetrahedral interstitial TI, hexagonal interstitial HI, ⟨110⟩ dumbbell interstitial DI, and ⟨110⟩ extended dumbbell interstitial EDI), calculated using two parametrizations of the SW potential (Refs. 29 and 37), the Tersoff (Ref. 38) and EDIP (Ref. 39) potentials, *ab initio* methods, and experimental data.

Si	V (eV)	SV (eV)	TI (eV)	HI (eV)	⟨110⟩ DI (eV)	⟨110⟩ EDI (eV)
SW (Original)	2.66	3.16	5.01	6.55	4.44	3.65
SW (Balamane)	2.83	3.80	5.29	6.83	4.48	3.92
Tersoff	3.70	3.54	3.60	4.64	4.43	3.85
EDIP	3.23	3.82	4.05	4.16	3.40	3.51
ab initio	3.49,[a] 3.53[b]		5.10[c]	3.80[c]	3.30,[d] 3.27[e]	
Experimental	2.40,[f] 2.8,[g] 3.6[h,i,j]		3.12[k]			

[a]Reference 15.
[b]Reference 17.
[c]Reference 40.
[d]Reference 20.
[e]Reference 41.
[f]Reference 42.
[g]Reference 43.
[h]Reference 1.
[i]Reference 3.
[j]Reference 44.
[k]Reference 45.

present here a brief complement of this review concerning the formation energy of the most common point defects known in silicon: the single vacancy (located on a given site or split between two) and the various possible interstitials (tetrahedral, hexagonal, ⟨110⟩ dumbbell and ⟨110⟩ extended dumbbell, see Fig. 1) for three of the most used potentials [SW,[29] Tersoff,[38] and one environment-dependent interatomic potential (EDIP) (Ref. 39)]. We have not included other mechanisms such as concerted exchange[5] because its migration energy barrier was found to be very high (~8 eV), at least with the SW potential.[4] The formation energies were calculated using systems of 512 ± 1 atoms (−1 for vacancies and +1 for interstitials) in cubic simulation boxes of sizes of 21.72 Å. The formation energy of the vacancy or the ⟨110⟩ extended dumbbell interstitial is obtained by equilibrating a system containing the considered point defect at high temperature (~1200 K), which is then quenched at 0 K by constrained molecular dynamics. In the case of the split vacancy, the relaxation is performed by keeping fixed the position of an atom at the saddle point on the path diffusion and some atoms at ~10 Å from the point defect. The other point defects (dumbbell, tetrahedral, and hexagonal interstitials) were directly located at a crystal site.

We present in Table I the formation energies of the point defects the most currently found in the literature. All these defects, including the hexagonal interstitial, are found either stable or metastable within our calculations (relaxation at 0 K by constrained molecular dynamics), except the splitted vacancy which is unstable but is shown here in relation with its saddle-point character during vacancy diffusion. Results are compared to those obtained by *ab initio* methods and experimental values when available.

The first important information that one can get from this table is the unability of the Tersoff potential to stabilize the vacancy with respect to the split vacancy. The SV corresponds to the diffusing atom occupying the transition state for vacancy migration. According to the first-principles calculations performed by Centoni *et al.*,[46] this position should be unstable for a neutral vacancy. The EDIP potential leads to a somehow intermediate situation in the sense that one recovers the stability of the vacancy but the SV is now metastable instead of being a saddle point; the saddle-point position being found between the unsplit and split situations. For these reasons we decided to use in this work the SW potential, even though it overstabilizes the vacancy with respect to the different interstitials when compared to *ab initio* values. On the other hand, the preferential creation of vacancies instead of interstitials is not a peculiarity of the SW potential but a more general trend of the empirical potentials, which contrasts to the *ab initio* methods. This is not, as can be thought, due to the unability of empirical potentials to account for Jahn-Teller distortion[24] around the vacancy because this effect would still lower the vacancy formation energy and enhance its stability.

III. SELF-DIFFUSION IN BULK SILICON USING SW POTENTIAL

A. Equilibrium defect concentration: Formation energy and entropy

As already mentioned, for the SW potential the formation energy of a vacancy is lower than the formation energies of the interstitials (see Table I). The lowest energy for interstitials corresponds to the ⟨110⟩ extended dumbbell, which is a pair of atoms occupying a single site of the original lattice and which extends to two nearest neighbors (see Fig. 1).[6] In the following, we will only consider the vacancy and the

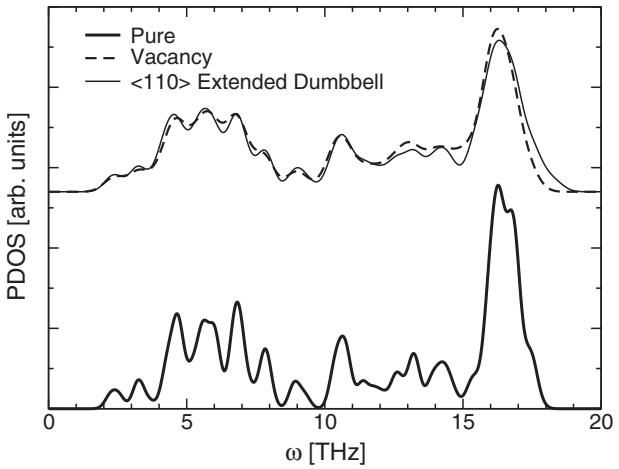

FIG. 2. Projected vibrational DOS averaged on the sites close to the defect ($i \in V^{\mathrm{def}}$) for a system containing either a vacancy (dashed line) or an ⟨110⟩ extended dumbbell interstitial (thin line). The DOS for a perfect system (bold line) is also shown. The curves have been shifted for the sake of clarity.

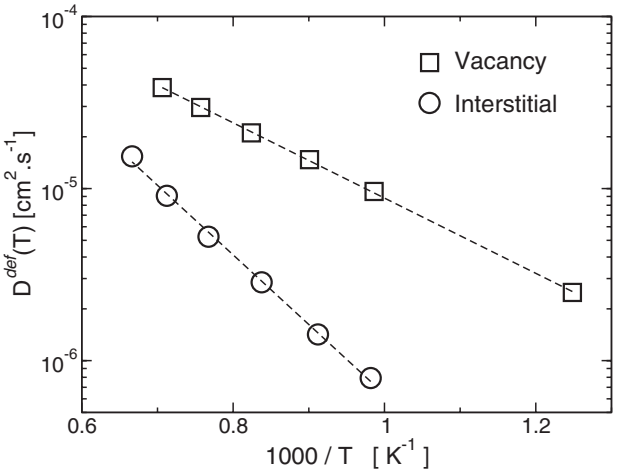

FIG. 3. Arrhenius plot of the diffusivity coefficient $D^{\mathrm{def}}(T)$ for the vacancy (squares) and the interstitial (circles), from which we extract the migration energy ΔE_m and prefactor D_m.

⟨110⟩ extended dumbbell interstitial which appear with the highest concentrations. All other defects, with lower concentrations, will be neglected. Before concluding about the respective concentrations of vacancies and interstitials in equilibrium, it is necessary to calculate the vibrational formation entropy. Following the method described in Sec. II A we calculate the local phonon densities of states in the perfect and defective systems including either a vacancy or an ⟨110⟩ extended dumbbell interstitial. The results are shown in Fig. 2 where the vibrational density of states is averaged on the sites close to the defect, which corresponds to roughly three shells around the defect ($Z^V=40$ and $Z^I=46$ sites for vacancy and ⟨110⟩ extended dumbbell, respectively).

Although it is not easily seen from the comparison of the three densities of states, the calculation of their average frequencies [Eqs. (8) and (9)] reveals that the introduction of the defects induces a shift toward lower frequencies $\bar{\nu}^V = 11.0$ THz and $\bar{\nu}^I = 11.3$ THz with respect to perfect bulk $\bar{\nu}^0 = 11.4$ THz. The larger shift in the case of vacancies can be related to the existence of larger zones with a tensile stress in the former and compensating zones with a compressive stress in the latter. One then expects an enhanced vibrational formation entropy for the vacancy.[47] This is confirmed by performing either the full calculation using Eq. (7) which gives $\Delta S^V_{f,\mathrm{vib}} = 4.3k_B$ and $\Delta S^I_{f,\mathrm{vib}} = 2.3k_B$ or the average frequencies and Eq. (10) which leads to $\Delta S^V_{f,\mathrm{vib}} \simeq 4.3k_B$ and $\Delta S^I_{f,\mathrm{vib}} = 1.7k_B$. Taking also into account the configurational contribution to the formation entropy, we obtain a total formation entropy of $(\ln 1+4.3)k_B = 4.3k_B$ for the vacancy and of $(\ln 6+2.3)k_B = 4.1k_B$ for the interstitial. It enhances the stability of the vacancy with respect to the interstitial at all temperatures. These values compare fairly well to those obtained by Sinno *et al.*[28] using molecular simulations at high temperature and the same SW potential who find $\Delta S^V_{f,\mathrm{vib}} = 4.0k_B$ and $\Delta S^I_{f,\mathrm{vib}} = 1.6k_B$. Comparison to other works in the literature is made difficult because most of them use an indirect method to calculate the formation entropy from other contributions, for example, using the SW potential and a different procedure: Maroudas and Brown[7] and Sinno *et al.*[28] reported values between $2k_B$ and $8k_B$ for the interstitial. In the case of interstitials, Tang *et al.*[40] use a tight-binding model to calculate the formation energy ΔE^I_f, the migration energy ΔE^I_m, and prefactor D^I_m and estimate the formation entropy $\Delta S^I_f \simeq 11.2k_B$ by fitting experimental values. Using local harmonic approximation and density-functional theory (DFT)-based calculations Blochl *et al.*[13] estimated the formation entropy of vacancies to be of the order $9k_B$. As a conclusion, from the point of view of the formation energy and entropy, the vacancy is more stable than the interstitial whatever the temperature, but the relative stability decreases when T increases.

B. Individual atom diffusivity: Migration energies and prefactors

The calculations have been performed using molecular dynamics at different temperatures on systems containing either 511 atoms (vacancy) or 513 atoms (interstitial) in a cubic box. The thermal-expansion coefficient κ was evaluated by performing constant pressure runs in a defect free system of 512 atoms at zero pressure and a temperature range going from 0 to 1600 K. We find an almost constant value of $\kappa = 3.81 \times 10^{-6}$ K^{-1} for temperatures between 0 to 700 K and a linear dependence at higher temperatures $\kappa = 4.25 \times 10^{-6}$ K^{-1} $- 6.76 \times 10^{-10}$ K^{-2}T.

First the system has been equilibrated at different temperatures in the canonical ensemble (NVT) from 800 to 1400 K for a vacancy and from 1000 to 1500 K for an interstitial, during 0.1 ns using a time step of 2 fs. In order to obtain two independent sets of data for each defect, two runs with different random numbers sets have been performed during the NVT equilibration of the system. Then, the dynamics has been continued in the microcanonical ensemble (NVE) during 20 ns to accumulate statistics of the square displacements, from which the diffusivity $D^{\mathrm{def}}(T)$ has been calculated using Eq. (15). The values of $D^{\mathrm{def}}(T)$ for the different temperatures have been plotted as a function of $1/T$ (see Fig. 3)

TABLE II. Migration energy and diffusivity prefactor D_m for a single vacancy and a single interstitial. SW refers to calculations using the Stillinger-Weber potentials (original parametrization) and TB to those using a tight-binding formalism.

Si	E_m^V (eV)	E_m^I (eV)	D_m^V (cm^2/s)	D_m^I (cm^2/s)
SW (dynamic) *this work*	0.43	0.84	1.53×10^{-3}	1.05×10^{-2}
SW (static) *this work*	0.49		4.19×10^{-3}	4.21×10^{-3}
SW	0.43,[a] 0.46[b]	0.90,[a] 0.94[b]	$1.50-1.70\times10^{-3}$ [a,b]	$1.60-1.76\times10^{-2}$ [a,b]
TB	0.10[c]	1.37[c]	1.18×10^{-4} [c]	1.58×10^{-1} [c]
ab initio	0.40[d]	0.45[e]	3.14×10^{-3} [d]	5.18×10^{-3} [e]
Experimental	0.40–1.40[f]			

[a]Reference 48.
[b]Reference 28.
[c]Reference 40.
[d]Reference 26.
[e]Reference 27.
[f]Reference 49.

in order to extract the migration energy ΔE_m and the prefactor D_m.

The migration energies and prefactors obtained using this procedure are summarized in Table II. For comparison we also report the static migration energy in the case of vacancies and static prefactors for vacancies and interstitials calculated using Eq. (14) and correlation factors taken from Ref. 9. As can be seen, the latter estimation gives the right order of magnitude (a few 10^{-3} cm^2/s) but is too crude to distinguish both mechanisms. Moreover, all these values are in good agreement with other results in the literature and with experimental results.[49,50]

From these results, it appears that the diffusivity mediated by either vacancies or interstitials obeys the well-known compensation law[51] according to which the prefactor somewhat compensates the diffusion barrier. As a consequence, it is reversed as a function of temperature. At $T<2500$ K the vacancy migrates faster than the interstitials and slower at $T>2500$ K.

C. Total self-diffusion

The previous analysis of the various contributions suggests that two different behaviors could exist depending on temperature. At low temperature, it is clear that self-diffusion is mediated by vacancies since they are more numerous and faster than interstitials. At high temperature the situation is more intricate since the stability of the vacancy with respect to interstitial decreases, the latter migrating now faster, leading to a competition between both mechanisms. In order to determine whether this competition should even lead to a reversal at sufficiently high temperature, it is necessary to get the overall dependence in temperature of the self-diffusion coefficient. To this aim, we have to combine both activation entropic and energetic contributions

$$D^{\mathrm{def}}(T) = \exp\left[\frac{\Delta S_a^{\mathrm{def}}}{k_B}\right]\exp\left[-\frac{\Delta E_a^{\mathrm{def}}}{k_B T}\right], \tag{16}$$

where the activation self-diffusion energy and entropy are given by

$$\Delta E_a^{\mathrm{def}} = \Delta E_f^{\mathrm{def}} + \Delta E_m^{\mathrm{def}}, \tag{17}$$

$$\begin{aligned}\Delta S_a^{\mathrm{def}} &= \Delta S_{f,\mathrm{vib}}^{\mathrm{def}} + \Delta S_{f,\mathrm{conf}}^{\mathrm{def}} + k_B \ln D_m^{\mathrm{def}} \\ &= \Delta S_{f,\mathrm{vib}}^{\mathrm{def}} + \Delta S_{f,\mathrm{conf}}^{\mathrm{def}} + \Delta S_{m,\mathrm{vib}}^{\mathrm{def}} + k_B \ln g^{\mathrm{def}} f^{\mathrm{def}} a^2 \nu_0^{\mathrm{def}}.\end{aligned} \tag{18}$$

These activation energetic [Eq. (17)] and entropic contributions [Eq. (18)] to the self-diffusion coefficient are derived from the values of the formation, migration, and configuration components calculated in Sec. II C, III A, and III B and summarized in Table III:

(i) Vacancy $\Delta E_a^V = 3.09$ eV, $\Delta S_a^V = -2.17 k_B$.
(ii) Interstitial $\Delta E_a^I = 4.49$ eV, $\Delta S_a^I = -0.46 k_B$.

The resulting behaviors of the vacancy and interstitial self-diffusion coefficients as a function of $1/T$ are shown in Fig. 4.

As can be seen, the two curves cross at very high temperature, revealing a transition from a vacancy-mediated diffusion at low temperature toward an interstitial-mediated one at high temperature. The critical temperature equals

$$T_c = \frac{\Delta E_a^V - \Delta E_a^I}{\Delta S_a^V - \Delta S_a^I}. \tag{19}$$

TABLE III. Summary of the formation and migration contributions calculated with the SW potential for the vacancy and the interstitial. In the third column is given the difference between the two defects.

	Vacancy	Interstitial	Vac.-Int.
$\Delta S_{f,\mathrm{conf}}^{\mathrm{def}}(k_B)$	0	1.79	−1.79
$\Delta S_{f,\mathrm{vib}}^{\mathrm{def}}(k_B)$	4.30	2.30	2.00
$k_B \ln D_m^{\mathrm{def}}(k_B)$	−6.47	−4.55	−1.92
$\Delta E_f^{\mathrm{def}}$ (eV)	2.66	3.65	−0.99
$\Delta E_m^{\mathrm{def}}$ (eV)	0.43	0.84	−0.41

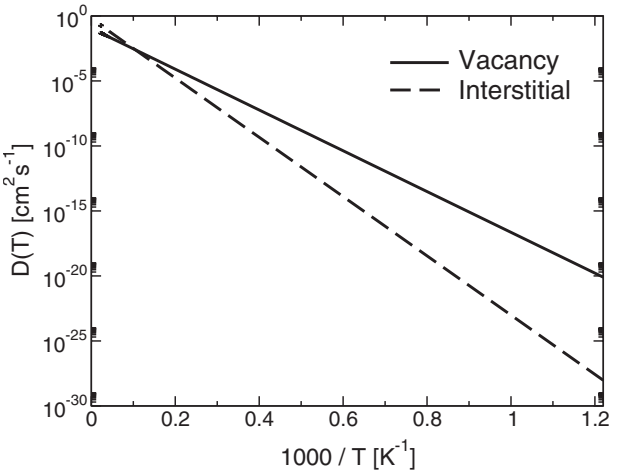

FIG. 4. Variation of the total diffusion coefficient as a function of the inverse of temperature for the vacancy and interstitial defects.

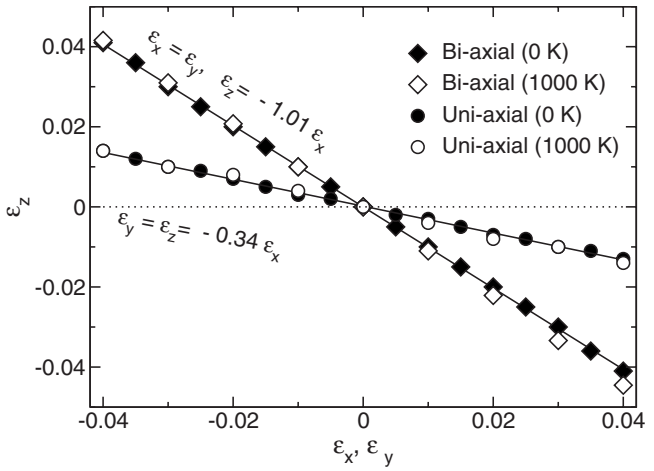

FIG. 5. ϵ_z deformation which cancels the stress in the z direction when applying biaxial deformations ϵ_x, ϵ_y (diamonds) and $\epsilon_{y,z}$ deformation which cancels the stress in the y,z direction when applying a uniaxial deformation ϵ_x at 0 K (circles). The closed symbols are the results at 0 K and the open ones at 1000 K.

Such a behavior is in qualitative agreement with the experimental observations which also predict a vacancy-mediated mechanism at low temperature and an interstitial-dominated one at high temperatures.[31,49,52–54] Unfortunately, our calculations are not able to reproduce the rather low order of magnitude of the experimental transition temperature (1200 K), since the Eq. (19) leads to an completely overestimated value of 9500 K.

This crude overestimation can be due to both energetic and entropic contributions. Indeed, it has already mentioned that the SW potential tends to underestimate the formation energy of vacancy, which according to Eq. (19) might increases T_c by a factor of 2–3. But this is not sufficient to account the difference of 1 order of magnitude found here. One has then to conclude that it is the difference between the entropic contributions of the two mechanisms which is underestimated in our calculation. A look at Table III reveals that the differences in migration and vibrational contributions almost perfectly compensate so that the total difference in entropy mainly comes from the configurational term. This is somewhat consistent with what would be guessed from the simplified Einstein formulation of Eq. (18)

$$\Delta S_a^V - \Delta S_a^I \approx \Delta S_{\text{conf}}^V - \Delta S_{\text{conf}}^I + k_B \ln\left(\frac{5}{6}\right) + (3Z-1)k_B \ln\left(\frac{\bar{\nu}^{I*}}{\bar{\nu}^{V*}}\right), \tag{20}$$

taking for simplicity the same $Z^{\text{def}}=Z$ for both defects. If in addition one assumes that the average frequencies at the saddle point do not differ too much, one finds

$$\Delta S_a^V - \Delta S_a^I \approx \Delta S_{\text{conf}}^V - \Delta S_{\text{conf}}^I - 0.19k_B = -1.98k_B.$$

The origin of our disagreement with the experimental temperature then remains to be elucidated. However, even though the crossover temperature is widely overestimated in our calculation this temperature dependence is a sign of the reliability of our potential. Indeed, from Eq. (19), it appears that the existence of a crossover requires for the differences in activation enthalpies and entropies to have the same sign. Since all calculations agree to find a negative sign for the entropy difference, this requires for the energetic term to follow the inequality

$$\Delta E_a^V < \Delta E_a^I, \tag{21}$$

which is clearly not the case for the values issued from *ab initio* calculations.[15,16,20,26,40,41,55,56]

IV. DIFFUSION UNDER EPITAXIAL STRAIN

We present here a study on the effect of a biaxial stress on the different quantities that participate in the calculation of the self-diffusion coefficients. A biaxial compressive or tensile stress mimics the stress suffered by a thin Si film deposited on a substrate with, respectively, a smaller or larger lattice parameter.

We suppose that the ⟨100⟩ directions of the crystal are aligned along the x, y, and z axis of the simulation box. Lateral deformations $\epsilon_x=\epsilon_y$ (from −4% to +4%) are applied isotropically along the [100] and [010] directions. Note that a deformation of +4% corresponds to a dilation of Si up to the lattice parameter of Ge. As we have used periodic boundary conditions along the three spatial directions to simulate a deposited film with a free surface in the z direction with a null component of the stress tensor σ_{zz} for each biaxial deformation $\epsilon_x=\epsilon_y$ we apply a deformation $\epsilon_z=-2\nu/(1-\nu)\epsilon_x$. The Poisson coefficient ν calculated for a perfect system has been used for the systems with defects. It has been determined at two temperatures (0 and 1000 K) in cubic simulation box with 512 atoms by performing biaxial and uniaxial deformations while relaxing in the perpendicular direction. In Fig. 5 we show the deformation ϵ_z which cancels the stress σ_{zz} when applying a biaxial deformation $\epsilon_x=\epsilon_y$ and the values of $\epsilon_z=\epsilon_y$ that cancel the stresses σ_{yy} and σ_{zz} when applying a uniaxial deformation ϵ_x. We consistently found the same Poisson ratio $\nu=0.34$, which compares fairly well

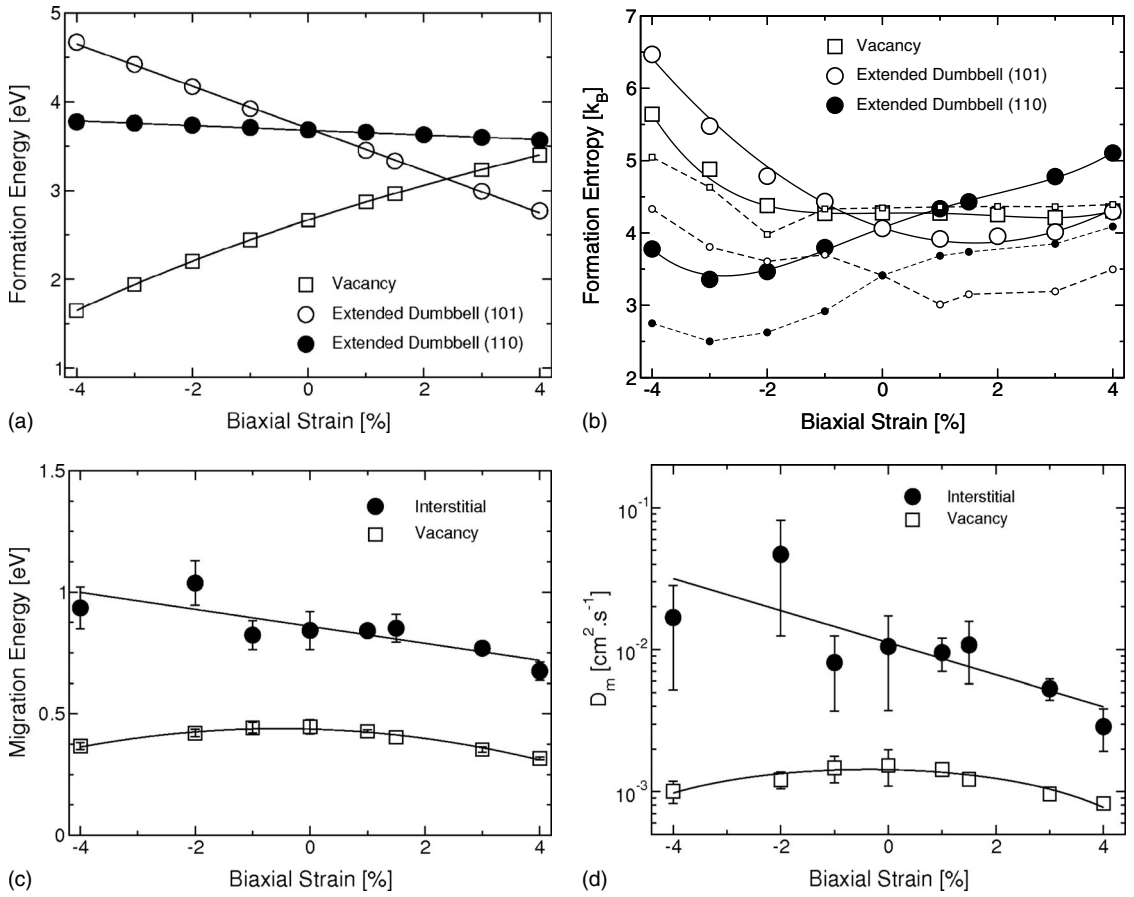

FIG. 6. Dependence of the (a) formation energy $\Delta E_f^{\mathrm{def}}$, (b) formation entropy $\Delta S_f^{\mathrm{def}}$, (c) migration energy $\Delta E_m^{\mathrm{def}}$, and (d) diffusivity prefactor D_m^{def} of vacancies and interstitials with the biaxial strain. In (b) the small symbols refer to the high-temperature approximation for the entropic contributions. The lines correspond to the polynomial laws which fit the various contributions.

to the experimental value of $\nu=0.28$.[57–59] As shown in Fig. 5, the Poisson ratio is almost independent of the temperature even though a very small deviation is observed for positive strain.

The formation and migration energies, the formation entropy, and the diffusivity prefactor associated to one or other point defects are calculated here using the same methodology as in the unstrained case. The variations of these four contributions to the total self-diffusion coefficient as a function of the deformation are shown separately in Fig. 6.

A. Equilibrium defect concentration: Formation energy and entropy under biaxial strain

Due to the anisotropic character of the biaxial strain applied, the defect orientation has to be taken into account when calculating the equilibrium defect concentrations (formation energy and entropy) under biaxial strain. In the case of a vacancy, no geometrical degeneracy is expected since the SW potential does not account for Jahn-Teller effect. The situation is different for ⟨110⟩ extended dumbbell interstitial which is an oriented point defect. We have then considered two types of ⟨110⟩ extended dumbbell interstitials, depending on that they are oriented in (110) and (101) planes. In the next, such interstitials are called (110) and (101) extended dumbbell interstitials to differentiate orientation.

In the energetic or entropic balances involved in the calculation of the formation quantities, the atom which is added or removed has been taken from or expelled to a site belonging to a bulk (reservoir) which undergoes the same deformation as the film.

Concerning the energetic part, the overall effect of the biaxial strain is to reduce the formation energy of the interstitial whatever its orientation and to increase that of the vacancy [see Fig. 6(a)]. This leads to a crossover at 2.5% which reverses the respective stabilities of the vacancy and of the (101) extended dumbbell interstitial, which is preferred to the (110) one under tensile strain.

These behaviors are quite natural since the creation of an interstitial (respectively, a vacancy) induces locally a compressive (respectively, tensile) stress which is reduced (respectively, increased) under dilation. The consequence is that it is easier to create an interstitial than a vacancy in a dilated lattice.

The effect of strain on the entropic part is even more complicated [see Fig. 6(b)]. For both the vacancy and the (101) interstitial, a compressive stress enhances the formation entropy while almost no effect is observed under a tensile stress, whereas for the (110) interstitial the formation entropy continuously increases from −3% to +4%. These different behaviors are closely related to the corresponding

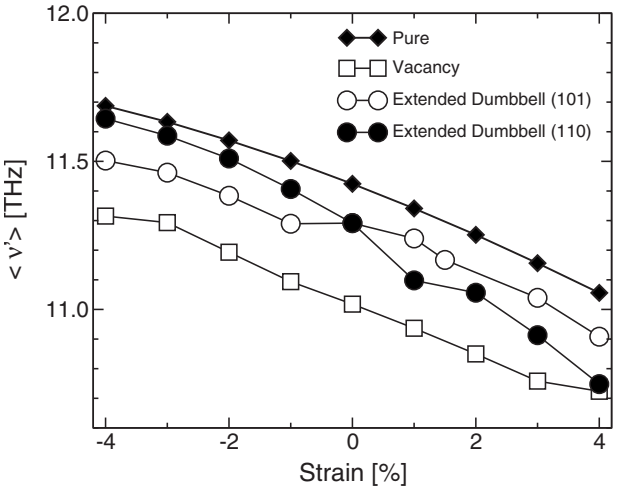

FIG. 7. Variation of the average phonon frequency as a function of the deformation for pure Si and in the vicinity of either a vacancy or an interstitial defect.

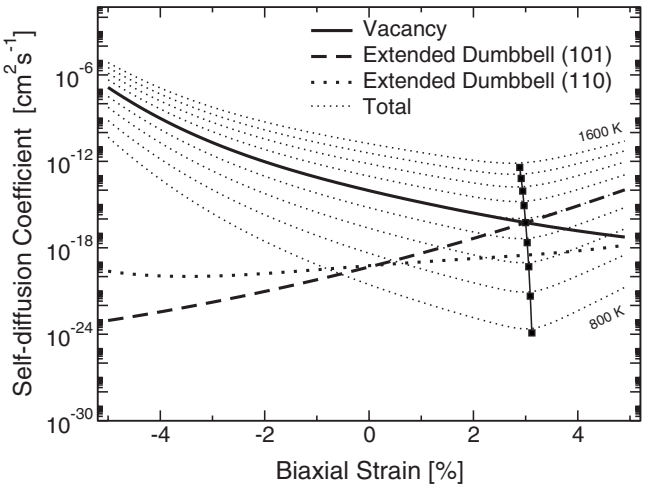

FIG. 8. Thick lines represent the variation of the self-diffusion coefficient mediated by vacancies (solid), (101) oriented (dashes), and (110) oriented (dotted) interstitials at 1200 K. Thin dotted lines account for the total self-diffusion coefficient resulting of the summation of these three mechanisms [Eq. (1)]. Vertical line with closed squares marks the crossover between contributions of (101) interstitials and vacancies.

variations of the phonon densities of states. Indeed, a dilation (respectively, a compression) induces an overall shift of the modes toward lower (respectively, higher) frequencies, which means that $\bar{\nu}^{\mathrm{def}}$ continuously decreases from −4% to +4% for both the perfect and defective lattices (see Fig. 7). As we have used a strained perfect system as the reference system, the variation of the formation entropies follows the differences between the evolution of the given defect and the pure system. This is confirmed by plotting, in Fig. 6(b), the high-temperature limit of the formation entropy which is directly related through Eq. (10) to the frequencies of the Fig. 7. As can be seen, this simplified formulation perfectly reproduces the overall behavior.

B. Individual atom diffusivity: Migration energies and prefactors under biaxial strain

As can be seen in Figures 6(c) and 6(d), both the migration energy and the prefactor present a weak dependence, which is quasiparabolic for the vacancies (with a maximum for unstrained Si), whereas it is slightly decreasing from −4% to +4% for the interstitials. These behaviors somewhat increase the difference between the two defects on the compressive side. Once again, it is tempting to relate the behavior of the prefactor [Fig. 6(d)] to that of $\bar{\nu}^{\mathrm{def}}$ through the high-temperature development [Eq. (14)]. From Fig. 7, it can be seen that, whatever the case (perfect lattice, vacancy, interstitial), $\bar{\nu}^{\mathrm{def}}$ decreases from compression to dilation, as expected from the associated shift toward lower frequencies of the corresponding vibrational densities of states. The same argument can be applied to understand why, for a given deformation, $\bar{\nu}^{V} < \bar{\nu}^{I}$, in qualitative agreement with the exact calculations.

C. Total self-diffusion under biaxial strain

In order to more easily analyze the dependence of the self-diffusion constants for the two oriented interstitials (which can be separated at least in what concerns their formation part) and the vacancy versus the temperature and the strain, we have fitted the variation of each contribution using a polynomial procedure in the temperature range (800–1600 K). The dependence with the biaxial strain for $T=1200$ K is shown Fig. 8. The first observation is that the strain dependence of the self-diffusion coefficient is opposite for the vacancy and interstitial mechanisms: it decreases from compression to dilation for the vacancy, whereas it decreases in the same time for the interstitial. A crossover occurs at this temperature at a deformation of about 3%, which means that diffusion is vacancy mediated below this deformation although the ⟨110⟩ extended dumbbell oriented along the (101) direction prevails beyond. One obviously recover that, as already mentioned in Sec. III C, the diffusion mechanism at zero deformation is vacancy mediated at this temperature. In addition, one observes a reorientation of the dumbbell from the (110) to (101) direction, when strain changes from compressive to tensile character. The behavior of the total diffusion coefficient is presented as thin dotted lines from 800 to 1600 K in Fig. 8. The transition from vacancy toward (101) dumbbell mechanism corresponds to the slope change which is marked with full points. As can be seen, the crossover is observed at each temperature at about the same value of tensile strain.

Although the range of absolute temperatures (800–1600 K) displayed above seems to be rather large, it remains rather narrow if one keeps in mind that our potential overestimates by 1 order of magnitude the transition temperature at which self-diffusion changes from vacancy toward interstitially mediated at zero strain ($T_c=9500$ K). In order to ensure the generality of our results, it is then more suited to consider scaled temperature T/T_c, in which case the range explored here becomes rather narrow (0.08–0.16). In order to access a wider range in T/T_c, we have interpolated the strain dependence of the formation and migration energetic and entropic

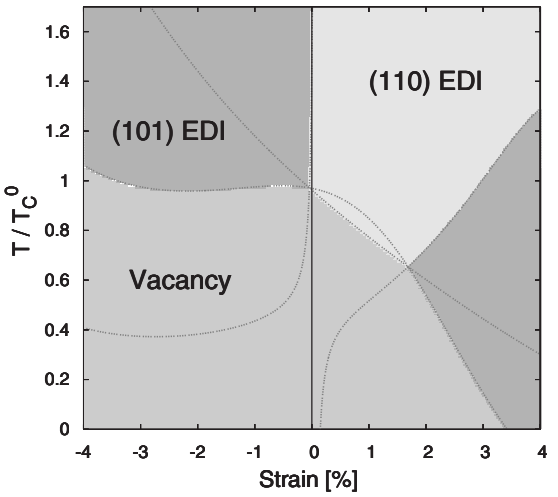

FIG. 9. (T,ϵ) diagram displaying the domains of existence of the vacancy and EDI mechanisms as a function of reduced temperature and strain. Colored domains correspond to the dominant mechanisms and the different lines represent the transitions between these mechanisms.

contributions using polynomial functions. The corresponding fits are displayed in Fig. 6. From these laws, we have been able to compare the respective efficiencies of the three mechanisms [vacancy, (101), and (110) oriented extended dumbbells] and then to derive analytic expression of the corresponding transition temperatures from one to the other mechanism by using extensions of Eq. (19). The corresponding transition lines are exhibited in Fig. 9 together with the domains of existence of the different mechanism. As can be seen, the situation on the tensile side is rather complex. One obviously recovers that at sufficiently low temperature, self-diffusion is governed by vacancies up to a critical strain of about 3% modifier (Si-Ge size mismatch) beyond which it is mediated by (101) oriented extended dumbbells. Then, for $T/T_c > 0.65$, the extended dumbbells change their orientation toward (110) and become more and more predominant with respect to vacancies up to $T/T_c = 0.65$, beyond which they are the only mechanism whatever the tensile strain. The situation on the compressive side is simpler. Indeed, the diffusion is found to be vacancy mediated whatever the compressive strain for $T/T_c < 1$ and governed by interstitials oriented in the (101) direction beyond. A simple way to summarize these results should be to say that although self-diffusion in bulk unstrained Si is governed by vacancies at low temperature, it becomes mediated by extended dumbbell under a critical dilation which can be either from thermal (increasing temperature) or from strain (biaxial stress) origin. Obviously, the absolute value of this critical dilation is potential dependent and it is overestimated by the SW one.

Finally, let us remark that our conclusions concern diffusion averaged in all directions. One can wonder on the anisotropy character of the migration contribution when it is calculated perpendicular or parallel to the biaxial deformation. To answer this question, we have analyzed separately the different components of the squared displacements at the limiting values of strain $\pm 4\%$. Under biaxial compressive strain (-4%), we have found that for interstitials they are almost equal in all directions whereas migration mediated by vacancies (dominant mechanism) is found to be $\sim 17\%$ larger in the direction perpendicular to the applied strain. Under tensile biaxial strain $(+4\%)$, self-diffusion is reduced in the direction perpendicular to the applied strain by a factor of 27% for the interstitials (dominant) and 15% for the vacancy one.

V. CONCLUSION

We have developed here a protocol to consistently calculate all the contributions to the self-diffusion coefficient in bulk Si using a unique interatomic potential. In this context, the Stillinger-Weber potential appeared the best suitable compromise. Using this potential, we have calculated the formation and migration energies and entropies for the vacancy and extended dumbbell interstitial which are the most stable defects for the SW potential. Our main result is that self-diffusion is essentially vacancy mediated at low temperature, whereas the interstitials should play a more important role at increasing temperature, in qualitative agreement with experimental observations. We have shown that a procedure involving only static calculations is able to reproduce the main features of the diffusion.

Using the same protocol, we have studied the effect of a biaxial strain on the self-diffusion. We have thus been able to build a general (T,ϵ) diagram which displays the domains of existence of the different mechanisms as a function of strain and temperature. The main features of this diagram are the following. At sufficiently high temperature, self-diffusion is mediated by the extended dumbbell interstitial, the orientation of which is driven by the sign of the strain. At lower temperature, it is governed by vacancies up to a critical dilation beyond which the extended dumbbell interstitial becomes the predominant mechanism. This critical dilation corresponds to Si-Ge size mismatch. Therefore, experimental conditions where a Si film grows pseudomorphicaly to a Ge substrate are expected to completely change the diffusion mechanism in the film with respect to bulk Si from vacancy- to interstitial-mediated diffusion. This last result should have important consequences when modeling nanoelectronic processes based on SiGe within TCAD-type codes.[60]

ACKNOWLEDGMENTS

This work was founded by the French National Agency ANR through OSiGeSim Project No. ANR-05-NANO-004. We thank all the partners of this consortium for enlightening discussions.

*ganster@cinam.univ-mrs.fr

[1] G. D. Watkins and J. W. Corbett, Phys. Rev. **134**, A1359 (1964).
[2] S. Mãkinen, H. Rajainmãki, and S. Linderoth, Phys. Rev. B **42**, 11166 (1990).
[3] P. Varotsos, K. Eftaxias, and V. Hadjicontis, Phys. Rev. B **38**, 6328 (1988).
[4] E. Kaxiras and K. C. Pandey, Phys. Rev. B **38**, 12736 (1988).
[5] E. Kaxiras and K. C. Pandey, Phys. Rev. B **47**, 1659 (1993).
[6] H. R. Schober, Phys. Rev. B **39**, 13013 (1989).
[7] D. Maroudas and R. A. Brown, Phys. Rev. B **47**, 15562 (1993).
[8] M. Posselt, F. Gao, and H. Bracht, Phys. Rev. B **78**, 035208 (2008).
[9] M. Posselt, F. Gao, and D. Zwicker, Phys. Rev. B **71**, 245202 (2005).
[10] L. A. Marqués, L. Pelaz, P. Castrillo, and J. Barbolla, Phys. Rev. B **71**, 085204 (2005).
[11] R. Car, P. J. Kelly, A. Oshiyama, and S. T. Pantelides, Phys. Rev. Lett. **52**, 1814 (1984).
[12] Y. Bar-Yam and J. D. Joannopoulos, Phys. Rev. Lett. **52**, 1129 (1984).
[13] P. E. Blöchl, E. Smargiassi, R. Car, D. B. Laks, W. Andreoni, and S. T. Pantelides, Phys. Rev. Lett. **70**, 2435 (1993).
[14] S. J. Clark and G. J. Ackland, Phys. Rev. B **56**, 47 (1997).
[15] A. Antonelli, E. Kaxiras, and D. J. Chadi, Phys. Rev. Lett. **81**, 2088 (1998).
[16] L. Mercer, J. S. Nelson, A. F. Wright, and E. B. Stechel, Modell. Simul. Mater. Sci. Eng. **6**, 1 (1998).
[17] A. F. Wright, Phys. Rev. B **74**, 165116 (2006).
[18] B. Sadigh, T. J. Lenosky, S. K. Theiss, M.-J. Caturla, T. Diaz de la Rubia, and M. A. Foad, Phys. Rev. Lett. **83**, 4341 (1999).
[19] W.-K. Leung, R. J. Needs, G. Rajagopal, S. Itoh, and S. Ihara, Phys. Rev. Lett. **83**, 2351 (1999).
[20] R. J. Needs, J. Phys.: Condens. Matter **11**, 10437 (1999).
[21] W. Windl, M. M. Bunea, R. Stumpf, S. T. Dunham, and M. P. Masquelier, Phys. Rev. Lett. **83**, 4345 (1999).
[22] J.-W. Jeong and A. Oshiyama, Phys. Rev. B **64**, 235204 (2001).
[23] X.-Y. Liu, W. Windl, K. M. Beardmore, and M. P. Masquelier, Appl. Phys. Lett. **82**, 1839 (2003).
[24] O. K. Al-Mushadani and R. J. Needs, Phys. Rev. B **68**, 235205 (2003).
[25] G. M. Lopez and V. Fiorentini, Phys. Rev. B **69**, 155206 (2004).
[26] F. El-Mellouhi, N. Mousseau, and P. Ordejón, Phys. Rev. B **70**, 205202 (2004).
[27] B. Sahli and W. Fichtner, Phys. Rev. B **72**, 245210 (2005).
[28] T. Sinno, K. Jiang, and R. A. Brown, Appl. Phys. Lett. **68**, 3028 (1996).
[29] F. H. Stillinger and T. A. Weber, Phys. Rev. B **31**, 5262 (1985).
[30] J.-R. Manning, *Diffusion Kinetics for Atoms in Crystals* (Van Nostrand, Princeton, 1968), p. 75.
[31] H. Mehrer, *Diffusion in Solids: Fundamentals, Methods, Materials, Diffusion-Controlled Processes* (Springer, New York, 2007), p. 116.
[32] G. Henkelman, B. P. Uberuaga, and H. Jónsson, J. Chem. Phys. **113**, 9901 (2000).
[33] G. T. Barkema and N. Mousseau, Comput. Mater. Sci. **20**, 285 (2001).
[34] G. H. Vineyard, J. Phys. Chem. Solids **3**, 121 (1957).
[35] A. M. Monti and E. J. Savino, Phys. Rev. B **23**, 6494 (1981).
[36] Y. Adda and J. Philibert, *La Diffusion Dans les Solides* (Press Universitaires de France, Paris, 1966).
[37] H. Balamane, T. Halicioglu, and W. A. Tiller, Phys. Rev. B **46**, 2250 (1992).
[38] J. Tersoff, Phys. Rev. B **39**, 5566 (1989).
[39] M. Z. Bazant, E. Kaxiras, and J. F. Justo, Phys. Rev. B **56**, 8542 (1997).
[40] M. Tang, L. Colombo, J. Zhu, and T. Diaz de la Rubia, Phys. Rev. B **55**, 14279 (1997).
[41] C. Z. Wang, C. T. Chan, and K. M. Ho, Phys. Rev. Lett. **66**, 189 (1991).
[42] J. A. Van Vechten, Phys. Rev. B **33**, 2674 (1986).
[43] V. Ranki and K. Saarinen, Phys. Rev. Lett. **93**, 255502 (2004).
[44] S. Dannefaer, P. Mascher, and D. Kerr, Phys. Rev. Lett. **56**, 2195 (1986).
[45] R. Vaidyanathan, M. Y. L. Jung, and E. G. Seebauer, Phys. Rev. B **75**, 195209 (2007).
[46] S. A. Centoni, B. Sadigh, G. H. Gilmer, T. J. Lenosky, T. Diaz de la Rubia, and C. B. Musgrave, Phys. Rev. B **72**, 195206 (2005).
[47] I. Meunier, G. Tréglia, R. Tétot, J. Creuze, F. Berthier, and B. Legrand, Phys. Rev. B **66**, 125409 (2002).
[48] G. H. Gilmer, T. Diaz de la Rubia, D. M. Stock, and M. Jaraiz, Nucl. Instrum. Methods Phys. Res. B **102**, 247 (1995).
[49] Y. Shimizu, M. Uematsu, and K. M. Itoh, Phys. Rev. Lett. **98**, 095901 (2007) and references therein.
[50] G. D. Watkins, J. R. Troxell, and A. P. Chatterjee, in *Defects and Radiation Effects in Semiconductors*, edited by J. H. Albany (Institute of Physics, London, 1978), Chap. 1, pp. 16-30.
[51] W. Meyer and H. Neldel, Z. Tech. Phys. (Leipzig) **12**, 588 (1937).
[52] H. Bracht, E. E. Haller, and R. Clark-Phelps, Phys. Rev. Lett. **81**, 393 (1998).
[53] H. A. Bracht, H. H. Silvestri, and E. E. Hallerb, Solid State Commun. **133**, 727 (2005).
[54] T. Y. Tan and U. Gosele, Appl. Phys. A: Solids Surf. **A37**, 1 (1985).
[55] D. Caliste and P. Pochet, Phys. Rev. Lett. **97**, 135901 (2006).
[56] Y. Kumeda, D. J. Wales, and L. J. Munro, Chem. Phys. Lett. **341**, 185 (2001).
[57] J. J. Wortman and R. A. Evans, J. Appl. Phys. **36**, 153 (1965).
[58] R. Zhu, E. Pan, P. W. Chung, X. Cai, K. M. Liew, and A. Buldum, Semicond. Sci. Technol. **21**, 906 (2006).
[59] A. George, in *Properties of Crystalline Silicon*, edited by R. Hull, EMIS Datareviews Vol. 20 (IEEE, New York, 1997), pp. 98.
[60] W. Fichtner, J. Comput. Theor. Nanosci. **5**, 1089 (2008).